Journal of Alloys and Compounds 509 (2011) L221–L227

Contents lists available at ScienceDirect

Journal of Alloys and Compounds

journal homepage: www.elsevier.com/locate/jallcom

Letter

Amphiphilic and photocatalytic behaviors of TiO_2 nanotube arrays on Ti prepared via electrochemical oxidation

Xianwu Zeng, Yong X. Gan*, Evan Clark, Lusheng Su

Department of Mechanical, Industrial and Manufacturing Engineering, College of Engineering, 2801 W. Bancroft Street, University of Toledo, Toledo, OH 43606, USA

ARTICLE INFO

Article history:
Received 23 January 2011
Available online 5 April 2011

Keywords:
TiO_2 nanotube arrays
Amphiphilic behavior
Photocatalysis
Self-cleaning
Electrochemical oxidation

ABSTRACT

Amphiphilic TiO_2 nanotube arrays (TiO_2 NTs) were fabricated through electrochemical oxidation of Ti in solution containing H_3PO_4 and NaF. Scanning electron microscopic analysis shows that the as-prepared TiO_2 NTs have an average pore diameter of 100 nm and a wall thickness of 15 nm. The electrochemical oxidation of Ti can be divided into four stages. In the first stage, when the potential is very low, oxygen formation and Ti dissolution are the major reactions. The second stage corresponds to a slightly higher potential, but less than 2.5 V. In this stage, the formation of TiO_2 film occurs. When the potential is increased to the even higher range from 2.5 V to 6 V, the TiO_2 film dissolves and nanoporous surface structure is generated. This is the third stage. Further increase of the potential enters stage four. The high potentials cause the self-organization of the nanostructure and allow the formation of well-aligned TiO_2 NTs. We also found that the change in surface condition of Ti by annealing heat treatment affects the film dissolution kinetics. As compared with TiO_2 thin film, the TiO2 NTs show higher photocatalytic activity on decomposing Rhodamine B. The surface of the TiO_2 NTs can be wetted by both water and oil. Such an amphiphilic property comes from the capillary effect of the nanochannel structure of the TiO_2 NTs. Because of the amphiphilic property and the photocatalytic activity, we conclude that the TiO_2 NTs have the capability of self-cleaning.

1. Introduction

Since titanium dioxide (TiO_2) was found to be useful as photo-catalyst for hydrogen generation [1], more and more semiconductor materials have been research for use as photo-catalysts. These include Fe_2O_3, NiO, WO_3 [2], ZnO [3], SnO_2 [4], ZrO_2, CdS [5] etc. Among all these photo-catalysts, TiO_2 is the best one because it has chemical stability and excellent charge transport property. It is also nontoxic and is an n-type semiconductor material. The band gap of solution-prepared regular TiO_2 is over 3.0 eV. TiO_2. Preparing TiO_2 with high temperature annealing results in an anatase structure with a bandgap of about 3.2 eV. Typically, pure TiO_2 can only absorb ultraviolet (UV) radiation, which accounts for only about 5% of solar energy.

Self-cleaning glass is a very important product which is based on the photo-catalytic property of a thin layer on the substrate. Nano-structured TiO_2 deposited at the surface of a flat glass shows self-cleaning behavior [6,7]. Normally, the glass surface is hydrophobic. After the TiO_2 thin film is added, the surface becomes hydrophilic. When the coated glass is exposed to sunlight, which contains UV radiation, the TiO_2 reacts with oxygen and water molecules present in the atmosphere to produce free radicals leading to oxidative species. These radicals have much higher energy than that of the covalent bonds between the organic material molecules. Thus the organic compounds can be decomposed into volatile molecules. These photo-catalytic and hydrophilic properties of TiO_2-coated glass allow rain to easily wash away the organic contaminants. The photo-Fenton waste water treatment system works under this mechanism. The photo-catalyst, TiO_2, helps decompose organic materials under UV radiation in the water [8,9].

The morphology of TiO_2 affects the efficiency of the photocatalysis. Up to now, most other researchers are using the self-cleaning glass containing a TiO_2 thin film as the photocatalyst. A mesoporous TiO_2 film photo-catalyst was prepared using the sol–gel method on a stainless steel substrate. Compared to conventional TiO_2 film photo-catalysts, the mesoporous TiO_2 film showed a better performance for the photo-degradation of rhodamine B (RB) solution and gaseous formaldehyde irradiated with UV light [10]. Recently, research on using TiO_2 nanotube arrays as photo-catalysts has been performed. For example, Shankar et al. [11] studied highly ordered TiO_2 nanotubes for water photoelectrolysis. Tan et al. [12] investigated the photocatalytic activity of TiO_2 in different forms including nanofilms, nanotubes (NTs) and nanotubes doped with Pd nanoparticles. Photodegradation of aqueous methylene blue (MB) solution and solid

* Corresponding author. Tel.: +1 419 530 6007; fax: +1 419 530 8206.
E-mail address: yong.gan@utoledo.edu (Y.X. Gan).

0925-8388/$ – see front matter © 2011 Elsevier B.V. All rights reserved.
doi:10.1016/j.jallcom.2011.03.154

stearic acid (SA) film under UV irradiation shows that the photocatalytic activity of TiO_2 from high to low can be ordered as: nanotube doped Pd nano-particles > pure nanotubes > nanofilms. It is found that, compared with raw TiO_2 particles, TiO_2 NTs have much higher specific surface area and pore volume. This greatly improves the photo-catalytic performance of the nanotubes [13].

Different methods have been developed for synthesizing TiO_2 NTs. These include sol–gel [14], microwave irradiation [15], hydrothermal processing [16], template synthesis [17] and electrochemical oxidation [18]. Among these, the electrochemical method, as introduced by Zwilling et al. in 1999 [19], is simplest. This method has caught more attention recently [20–29]. Basically, TiO_2 NTs grow on the surface of the anode of Ti foils or thin sheets. Several kinds of inorganic or organic solutions containing F^- ions can be used as electrolytes. For example, H_2SO_4/HF [20,21], H_3PO_4/HF [22], ethylene glycol/HF [23], glycerol/NH_4F [24,25], ethylene glycol/NH_4F [10,24,26], NaH_2SO_4/HF [27,28], and Na_2SO_4/NaF [29] have been used before. In this method, the size of the TiO_2 NTs can be controlled by adjusting electrochemical processing parameters [23,24].

Processing parameters have significant influence on the dimension of electrochemically formed TiO_2 NTs. For example, Sreekantan et al. [30] examined the effect of pH on the formation of titania nanotubes. The lengths of the nanotubes can be controlled in the range from 0.7 to 2.5 μm by altering the pH values of electrolytes containing Na_2SO_4 and NH_4F. In the work performed by Lockman et al. [31], influence of anodisation voltage on the dimension of titania nanotubes was examined. Zhao et al. [32] investigated the processing time effect. They prepared well-ordered nanotube arrays of titania with a length of up to 1.1 μm via constant-voltage experiments. It is found that the length of the nanotubes at first increases with the anodizing time and then reaches a maximum value due to a dynamic balance of titania formation and dissolution. However, the conditions under which TiO_2 thin films are converted into nanotubes have to be identified. That is why we performed the processing work as will be presented in the first part of the paper.

It is true that preparation of TiO_2 NTs through electrochemical oxidation is a well studied field. Nevertheless, the research on the amphiphilic behavior of the nanotubes has been much less studied. To the best of our knowledge, only a few papers reported the amphiphilic behavior of the nanotubes. For example, Song et al. prepared amphiphilic TiO_2 nanotube arrays [33]. But an intermediate procedure is needed to modify the surface properties of the nanotubes using octadedecylphosphonic acid (OPDA). The question remains to be answered is how amphiphilic TiO_2 nanotube arrays can be made in a more simplied way, for example, in the well established one-step electrochemical oxidation process. This provides us the motivation to make the fundamental studies on the super hydrophility of TiO_2 nanotube arrays as described in the last part of this paper.

In this work, we synthesized TiO_2 NTs through electrochemical oxidation using a much milder solution than previously used by other researchers. Our solution contains H_3PO_4 and low concentration of NaF. In order to evaluate the photo-catalytic activity of the prepared TiO_2 NTs, rhodamine B (RB) was used as the dye. A specific RB solution with the concentration of 25 ppm was prepared for the photo-degradation test. Under the same UV radiation conditions, the RB solution shows different degradation behaviors when the specially prepared TiO_2 NTs and the natually formed TiO_2 thin film are used as the photo-degradation anodes. To test the wettability with organic substances, a vegetable oil (specifically corn oil), was used. It is found that the TiO_2 NTs and TiO_2 thin film show different wetting abilities with the oil. The TiO_2 NT specimen has much higher affinity to the oil than the TiO_2 thin film.

2. Experimental

2.1. Materials and methods

The rhodamine B dye used was in fine powder form. A titanium (Ti) sheet (0.5 mm thickness, 99.99%) was used as the substrate material in order to form TiO_2 nantotube arrays. Orthophosphoric acid (H_3PO_4, 85 wt%) and sodium fluoride (NaF, powder, 99.99%) were used to make the electrolyte for anodic oxidation of the titanium. All of the above materials were purchased from Alfa Aesar. De-ionized (DI) water was used throughout the study.

The electrochemical oxidation was performed by the use of a regulated DC power source (model HY5003, 0–50 V, 0–3 A). A CHI 400A Electrochemical Work Station, purchased from CH Instrument, Austin, TX, was used to conduct cyclic voltammetric studies to determine the transition voltage at which TiO_2 thin films are converted into nanotubes. The ultraviolet lamp used was a UVL-21 lamp (365 nm UV, 4 W, 0.16 A). This lamp generated UV radiation for RB degradation. Quanta 3D FEG (FEI) electron microscope was used for observing the morphology of the TiO_2 nanotube arrays. A spectrometer (RED TIDE USB650 370–980 nm, Ocean Optics, Inc.) was used to measure the light absorption and transmission of RB after UV degradation. A ProScope HR (high resolution) USB hand-held microscope was used for taking optical micrographs during the wettability test.

2.2. Preparation of self-organized TiO_2 NTs

TiO_2 NTs were synthesized by electrochemical oxidation. Titanium (Ti) sheet was cut into 20 mm × 20 mm specimens. Before the electrochemical processing, the sheet was cleaned using de-ionized (DI) water. The electrolyte solution consisted of 1.0 M H_3PO_4 and 0.15 M NaF. Some researchers used a three-electrode electrochemical cell for the anodic oxidation [22,29]. But a two-electrode electrochemical cell was also found to have produced good quality titania nanotubes [23,26,27]. In this electrochemical experiment, anodic oxidation was performed in a simpler two-electrode cell at room temperature. The anode and the cathode are 20 mm × 20 mm Ti sheets. The distance between the two electrodes was about 40 mm. The operation voltage was 20.0 V and the processing time was 2 h. Other researchers have also used these conditions [27,34]. After anodic oxidation, the samples were washed by immersion in de-ionized water and air-dried. The surface of the anode was completely covered by TiO_2 nanotube arrays as revealed by the immediate morphological observation using the Quanta 3D FEG (FEI) electron microscope.

2.3. Rhodamine B (RB) photocatalytic degradation

The photo-catalytic degradation test was performed using a 15 ml 25 ppm RB solution. For the as-prepared TiO_2 nanotube arrays, the photo-catalytic anode with the same nominal area of the titanium plate, i.e. 20 mm × 20 mm, was immersed into the RB solution. While under UV radiation (UVL-21: 365 nm UV, 4 W, 0.16 A), the solution was checked by the spectrometer every 30 min. The intensity of the UV radiation was about 40 mW/cm^2. The distance between the UV light source and the TiO_2 nanotube array photo-catalytic anode was kept at 40 mm. For the preparation of the TiO_2 thin film specimen, a Ti sheet with the dimension of 20 mm × 20 mm was oxidized in air. The condition for RB degradation using the TiO_2 thin film specimen was the same as that of the TiO_2 nanotube array sample. The recorded data in the experiments include both absorbance and transmission of UV–visible light. After finishing the experiments, the two samples were washed by de-ionized water and air-dried.

2.4. Wettability experiment

Both water and oil dispersion on the TiO_2 nanotube arrays and TiO_2 thin film was tested. The same two samples as used for degradation of RB were adopted in this experiment. Specifically, the wettability of the corn oil to the two different substrates was studied. One drop of oil was put on the sample with TiO_2 nanotube arrays and another drop was put on the sample with TiO_2 thin film. The two samples were exposed to the same dosage of UV radiation (UVL-21, 40 mW/cm^2). Images recording the shape of the oil drops were captured by the ProScope HR microscope at various radiation periods. For comparison, a drop of oil was put on a glass slide during the experiment. After the radiation test, all the samples were cleaned.

3. Results and discussion

3.1. Morphology and growth mechanism of the TiO_2 nanotube array

At 20 V, the well-ordered TiO_2 nanotube arrays were formed on the surface of the anodic Ti sheet and hydrogen was released at the cathode. Fig. 1 shows the morphology of the TiO_2 thin film and the as-prepared TiO_2 nanotube arrays. Fig. 1(a) is a low magnification scanning electron microscopic (SEM) image showing the slightly oxidized surface of the titanium sheet. Some scratches and inden-

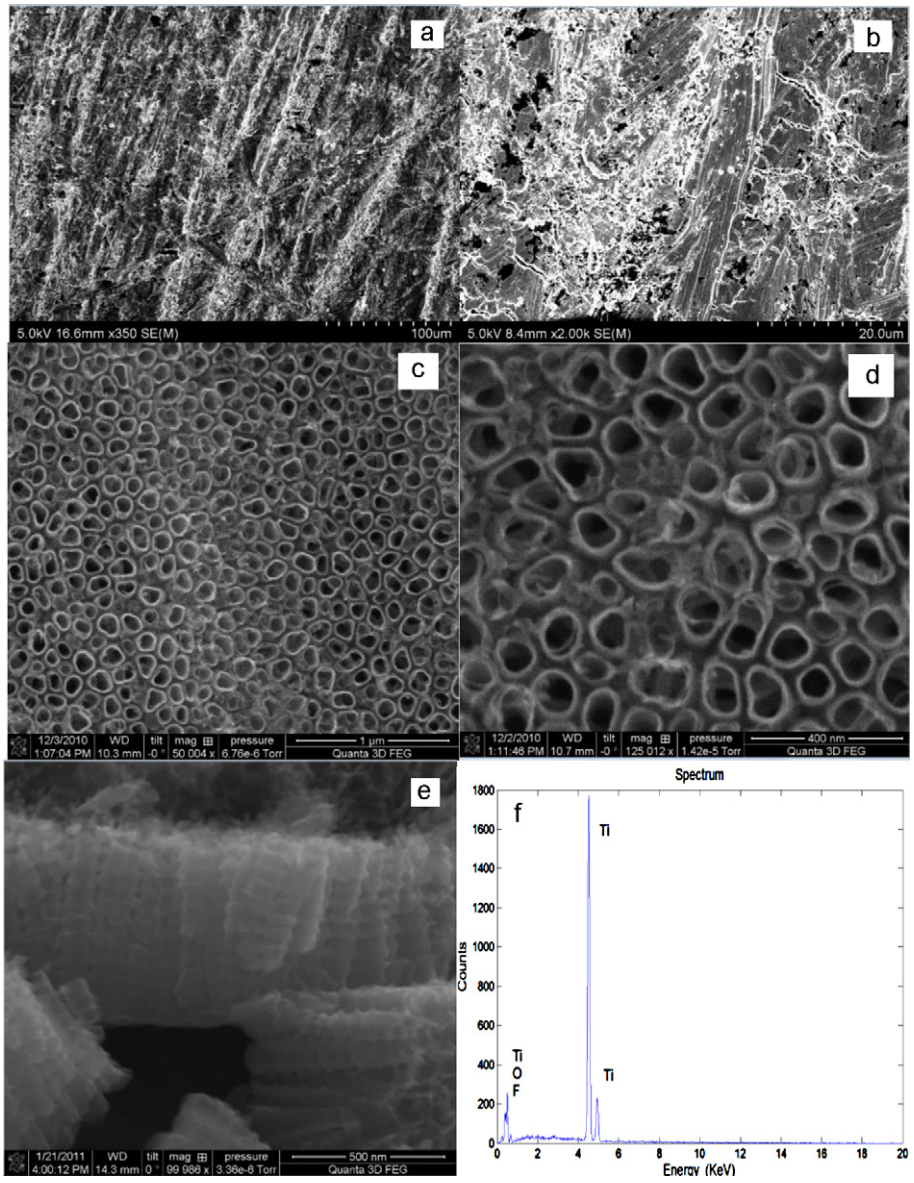

Fig. 1. SEM images showing the surface morphology of TiO_2 thin film, nanotube arrays and EDX spectrum of the nanotubes: (a, b) TiO_2 thin film on Ti; (c, d) TiO_2 nanotube arrays on Ti; (e) side view of the nanotube arrays and (f) EDX spectrum.

tations were found because no specific polishing of the Ti was made before the oxidation. In Fig. 1(b), at a slightly higher magnification, the oxide film was found to be pretty rough and some titanium oxide islands can be seen. Fig. 1(c) provides a global view of the TiO_2 nanotube arrays. At higher magnification, the nanotubes were found to be slightly squeezed into an elliptic shape.

Fig. 1(d) is a high magnification SEM image of the nanotubes. From Fig. 1(d), it can be estimated that the TiO_2 nanotubes have the average diameter of about 100 nm. The nanotube wall thickness is about 15 nm. These dimensions were obtained under the conditions of 20 V and 2 h anodic oxidation time in the electrolyte containing 1.0 M H_3PO_4 and 0.15 M NaF. If the voltage and time for the oxidation or the electrolyte composition were changed, the dimensions of the TiO_2 NTs could be changed, as indicated earlier in literature [20,26]. Fig. 1(e) shows the cross-section of the nanotube arrays. The energy dispersive X-ray (EDX) diffraction spectrum reveals that Ti and O are the major elements. The quantitative analysis shows that the atomic ratio of Ti to O is about 1–2, which is the composition of TiO_2. Some fluorine ions are encapsulated into the tubes and remain as an impurity.

The formation of nanotubes in an aqueous electrolyte containing fluorine ions follows the fundamental electrochemical principles. The Ti metal as the anode is oxidized and partially dissolved into the electrolyte. The growing mechanism of TiO_2 nanotube arrays may be found in references [11,23]. We have proposed a slightly different mechanism and the electrochemical processes follow the reactions as below:

$$\text{Oxygenformation}: \quad H_2O \rightarrow [O] + 2e^- + 2H^+ \tag{1}$$

$$\text{Titaniumoxidation}: \quad Ti \rightarrow Ti^{4+} + 4e \tag{2a}$$

$$Ti + 2[O] \rightarrow TiO_2 \tag{2b}$$

$$\text{Nanopore, nanotubeformation}: \quad TiO_2 + 6F^- + 4H^+ \rightarrow [TiF_6]^{2-}\, 2H_2O \tag{3}$$

$$\text{Hydrogengeneration}: \quad 2H^+ + 2e^- \rightarrow H_2\uparrow \tag{4}$$

Although these electrochemical reactions look like intuitive, the titanium oxide film was formed in what voltage range is still uncer-

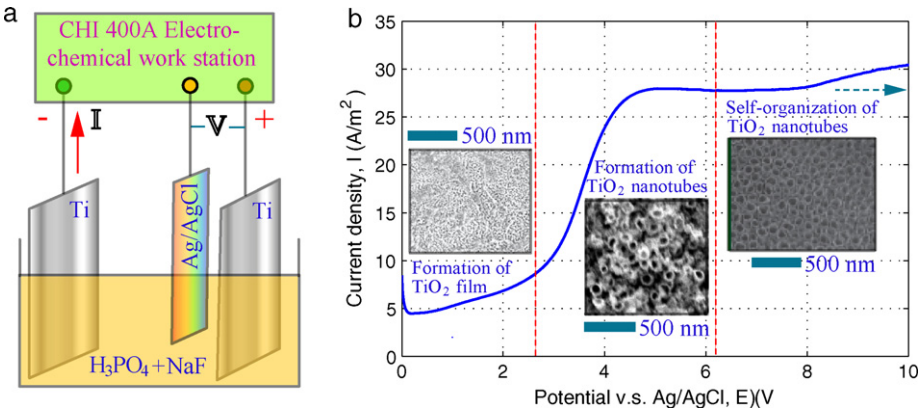

Fig. 2. Electrochemical reaction mechanism analysis experimental set-up and the results (a) cell configuration and (b) cyclic voltammetry and morphological examination results revealing various reaction stages.

tain. In addition, the voltage condition under which the solid TiO_2 thin film was converted into a porous structure remains to be identified. At what voltage value the porous film self-organizes into TiO_2 nanotubes is needed to be determined.

We dealt with these issues through the cyclic votammetry studies. Analysis of the cyclic voltammetrical data was combined with the morphology observation, which helps to reveal how the above electrochemical reactions happened. A three-electrode configuration as shown in Fig. 2(a) was used to generate potentail scans and cyclic voltammetry data were recorded. The data were ploted as current density, *I*, versus scan potential, *V*. In Fig. 2(b), the forward scan results are given. From the *I*–*V* curve in this figure, it is found that the electrochemical reaction as described by Eqs. (1) and (2a) occur at very low voltage values. Oxygen formation and Ti dissolution are the major events. The small peak close to the current density (*I*) axis corresponds to these reactions. The current density drops after this peak. This is the indication of Ti oxidation. That is, the reaction described by Eq. (2b) started. Since the formation of TiO_2 film on Ti due to the oxidation increases the electrical resistance, the current density decreases until the potential reaches the values higher than 2 V.

After passing this stage, it was believed that the dissolution of the TiO_2 film occurred at the potential values higher than 2.5 V, which means that the reaction described by Eq. (3) started besides Eqs. (1), (2a) and (2b). The dissolution of the film results in the formation of nanopores and nanotubes. The current density was increased a lot. At the cathode, the formation of hydrogen was observed; i.e. the reaction described by Eq. (4) also happened. If the potential is increased further to the range higher than 6 V, the self-organization of the porous TiO_2 nanostructure generated highly-ordered TiO_2 nanotubes. A dynamic balance between TiO_2 dissolution (as described by Eqs. (2a) and (3) and TiO_2 formation through Ti oxidation (as described by Eq. (1)) was reached. That is why the current density was kept almost constantly. Fig. 2(b) clearly shows all the above mentioned electrochemical reaction stages on the *I*–*V* curve. Also presented in this figure are the SEM image inserts. They nicely reveal the structures generated in the corresponding voltage ranges. The observed features on these SEM images show consistency with the reaction mechanism as reveal by the *I*–*V* curve.

From the above analysis, we deduce that the electrochemical oxidation of Ti can be divided into four stages. The first stage is characterized by the low applied potential and a relatively high current density. Oxygen formation and Ti dissolution happened. The second stage corresponds to the potential range of less than 2.5 V. In this stage, TiO_2 film forms and the current density drops down. When the potential is increased to the higher range from 2.5 V to 6 V, TiO_2 film dissolves and nanoporous surface structure is generated. This belongs to the third stage. Further increase of the potential enters stage four. The high potentials result in the self-organization of the nanostructure to form well-aligned TiO_2 NTs. The current density is almost at constant due to the dynamic balance is reached.

Specifically, the pore formation in the TiO_2 film was examined. Fig. 3(a), an SEM image shows the surface morphology of the

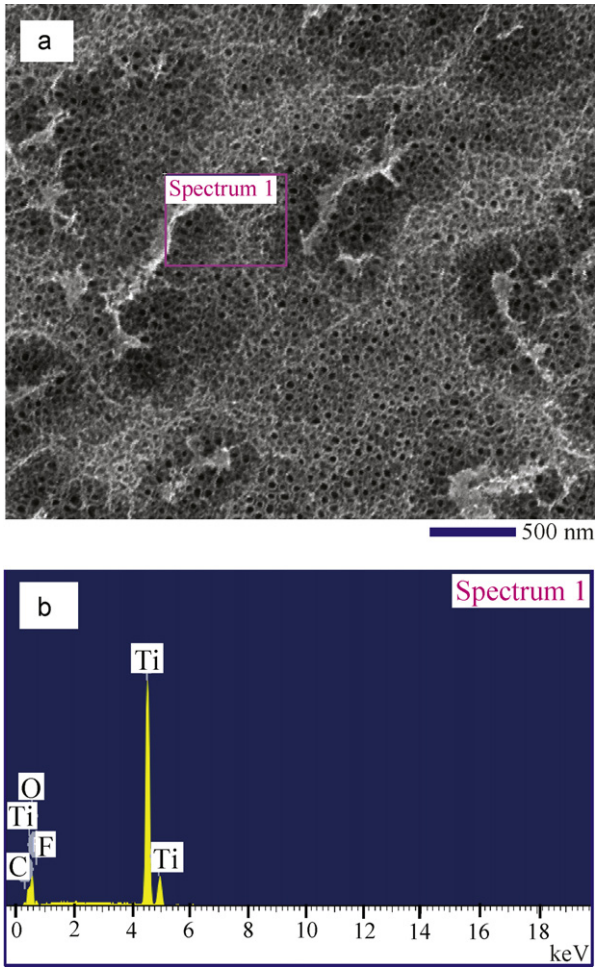

Fig. 3. Analysis of TiO_2 thin film dissolution: (a) SEM image showing the nanopore formation in the TiO_2 thin film and (b) EDX spectrum of the nanoporous film.

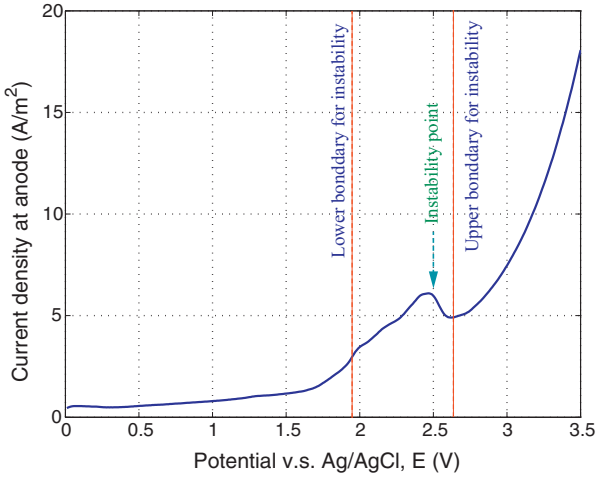

Fig. 4. Cyclic voltammetry of annealed Ti associated with the electrochemical oxidation.

anode after taken off from the electrolyte upon the electrochemical oxidation at 2.5 V. The TiO_2 film has a lot of pores. Elemental analysis using the energy dispersive X-ray (EDX) diffraction technique reveals Ti, O are the major elements as can be seen from Fig. 3(b). However, F was found due to the penetration of fluorine ions into the film at the positive scan potential. Trace amount of C was also shown, which was from the carbon type for holding the anode.

Comparative studies on the *I–V* characteristics of unannealed Ti and annealed Ti was also performed. The annealed Ti was heat treated at 500 °C for 2.5 h and cooled down naturally. After the annealing treatment, the Ti has colors due to the formation of the surface oxide layer. The annealed Ti with the surface oxide layer was electrochemically oxidized in the same H_3PO_4 + NaF electrolyte. Its *I–V* curve is shown in Fig. 4. The small peak close to the current density (*I*) axis as observed in Fig. 3(b) disappeared. The reason is that the pre-existing oxide film generated by annealing provided a high electrical resistance to the specimen and only allowed a very small current density at the very beginning of the potential scan. Interestingly, the breakage of this pre-existing oxide film is more obvious than the electrochemically formed oxide film on the unannealed Ti. This can be seen from Fig. 4 in the potential range from 2 to 2.5 V. On the *I–V* curve, the instability of current density can be seen around 2.5 V. This is due to the fast dissolutoin of the annealed film. While in Fig. 3(b), the the *I–V* curve for the unannealed Ti specimen does not shown only instability in current density at this potential level. Therefore, we conclude that the change in the surface condition of Ti due to heat treatment affects the film dissolution kinetics.

3.2. Rhodamine B (RB) degradation characterized by light transmission and absorption

Measurements of both light transmission and absorption of Rhodamine B (RB) were performed to characterize the photo-catalytic behavior of the nanotubes. Due to the photodecomposition of RB by the TiO_2 nanotubes, a change in the intensity of light transmission and absorption was observed. Fig. 5(a) schematically shows the light transmission and absorbance measurement system. The light transmission is defined as the portion of energy passing through the RB solution relative to the amount that passes through a reference sample. Transmission mode can also display the portion of light reflected from a sample since transmission and reflection measurements are related mathematically. Absorbance spectra measure how much light is absorbed. In most cases, the absorbance relates linearly to the concentration of the substance. This is known as Beer's Law. In this work, we used the Spectra Suite (RED TIDE USB650 370–980 nm) system to acquire the transmission and absorption data. The transmission and absorbance were then calculated following the associated formulae.

The light transmission measurement results are presented in Fig. 5(b). The unit for the intensity is measured by counts. It can be seen that RB can pass most of the light except the light with wavelengths ranging from 450 to 600 nm. This means that the

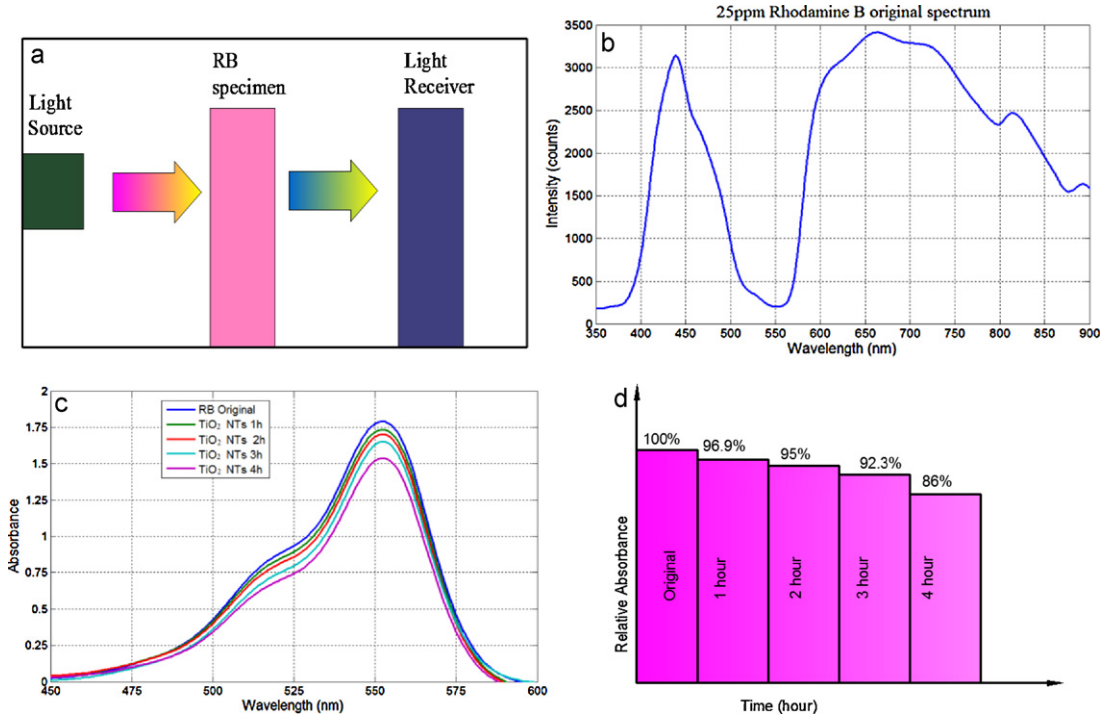

Fig. 5. Rhodamine B degradation spectra: (a) measurement system drawing; (b) light transmission spectrum of 25 ppm RB original solution without UV degradation; (c) absorbance spectra of RB after UV degradation and (d) relative absorbance intensity versus time.

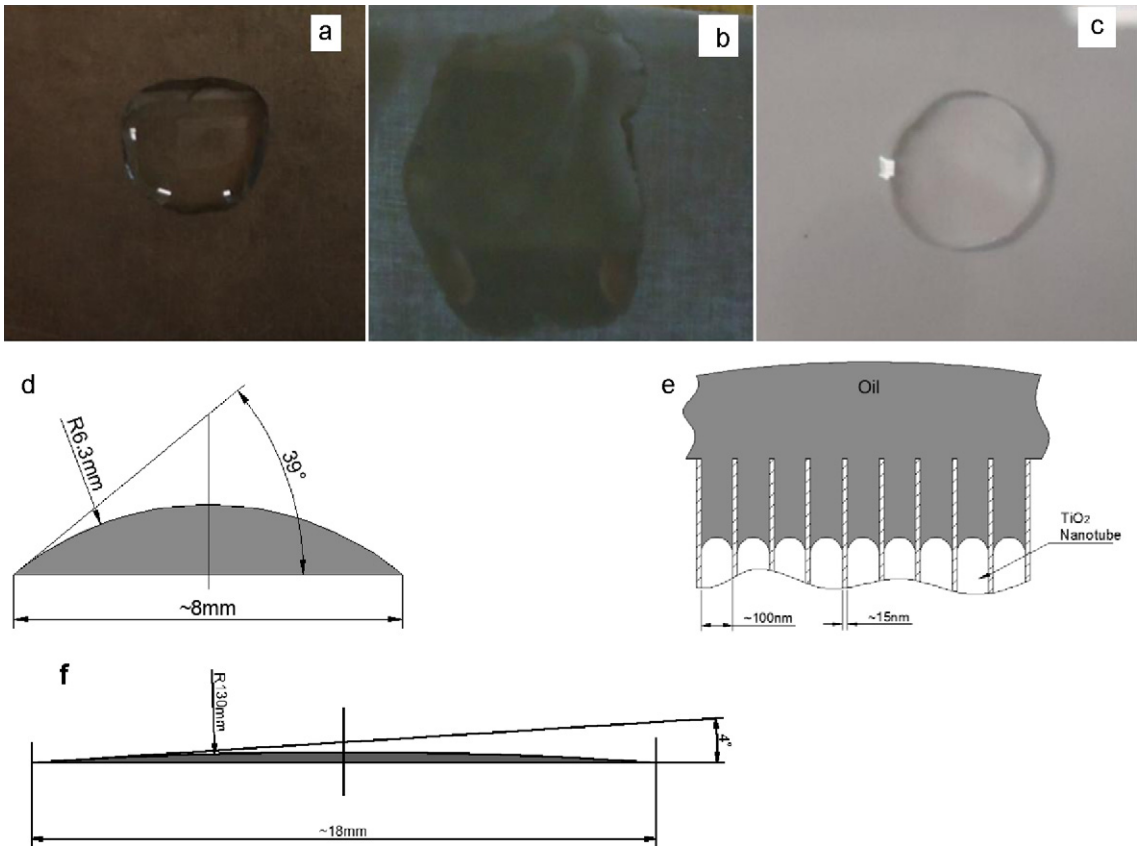

Fig. 6. Optical micrographs showing oil drops on different surfaces and the drawings of measured contact angles: (a) oil droplet on TiO_2 thin film surface; (b) oil droplet on TiO_2 NTs surface; (c) oil droplet on soda-lime glass surface; (d) schematic of oil droplet on TiO_2 thin film and soda-lime glass surface showing the same contact angle of 39°; (e) the capillarity schematic map of oil on TiO_2 NTs and (f) schematic of oil droplet on TiO_2 NTs showing the contact angle of 4°.

light within the specified wavelengths is absorbed by the RB solution. Time-dependent photo-degradation data was generated and plotted. Fig. 5(c) shows the degradation absorbance spectra of RB within 450–600 nm at different degradation time periods. It can be seen that, with the increasing UV radiation time, the absorbance becomes lower and lower. The reduction in the intensity at the peaks was examined. The results were plotted in a bar chart in Fig. 5(d). This figure shows the relative absorbance versus time. The longer the degradation time, the lower the light absorbance is. Such a trend reveals the obvious time-dependent photocatalytic activity of the TiO_2 NTs.

3.3. Amphiphilic and self-cleaning behaviors

Self-cleaning properties have many potential applications. For example, fluorine-doped tin oxide (FTO) glass is a good conductor that is widely used in solar cells. If TiO_2 NTs are deposited on FTO glass, there is no need to use any special cleaning process on solar cells. Pure titanium films can be deposited by radio frequency magnetron sputtering (RFMS) at room temperature on the surface of FTO glass. The TiO_2 NTs can be formed by anodic electrochemical oxidation in the NH_4F/glycerol electrolyte [35]. In the work performed by Chen et al. [20], it has been found that water drops show different wetting behaviors on the surface of both TiO_2 NTs and TiO_2 thin films. Water drops spread very quickly over the surface of the TiO_2 NTs even without UV radiation, but water drops on the TiO_2 thin film surface required UV radiation for at least several minutes before the contact angle decreased to zero. The TiO_2 NTs are super hydrophilic. Our experiments on water wetting tests are consistent with previous reported results [20].

Oil wetting tests were also performed to evaluate the amphiphilic property of the TiO_2 NT arrays and TiO_2 thin film. From these wetting tests, we found that the corn oil can only partially wet the TiO_2 thin film. However, it can completely wet the surface covered by TiO_2 NT arrays. Fig. 6 shows the oil drops on different surfaces. On the TiO_2 thin film, as shown in Fig. 6(a), the oil drop spreads out only slightly. In contrast, Fig. 6(b) shows that a corn oil drop spreads out completely across the surface containing the TiO_2 NT tube arrays. It does this very quickly even without the assistance of UV radiation. The super hydrophilic property of the TiO_2 NTs is known to be the capillary effect of the nanotubes [20]. Fig. 6(c) is an image of the oil drop on a soda lime glass slide. It can be seen in this figure that the oil drop just partly spreads out on the glass.

Quantitative analysis of the wettability of the oil on the surface of the TiO_2 thin film, NT arrays, and the soda lime glass was made. The contact angle measurements were repeated at least 5 times in order to obtain accurate quantitative results. The average values of the contact angles of the oil on the titanium oxide thin film and nanotube arrays from multiple measurements are presented. The results reveal that, due to the existence of the nanotubes, the wettability was enhanced. This is meaningful because a good wettability results in the effective photodecomposition of pollutants on the surface of the nanotubes. Fig. 6(d) is a schematic showing the contact angle of the oil droplet on the TiO_2 thin film and soda-lime glass surface. The contact angle was found to be 39° for corn oil on both substrates. If the oil drop is set on the TiO_2 NT arrays, a strong capillary effect as shown in Fig. 6(e) results in the oil being quickly sucked into the pores of these nanotubes. This causes the contact angle to be reduced dramatically. As shown in Fig. 6(f), the contact angle of the oil droplet on the TiO_2 NTs is about 4°. This behavior increases the contact area between the oil drops and the walls of

the nanotubes. Using UV radiation, the oil drop can be decomposed much faster by the nanotubes than by the thin film of TiO_2.

From both qualitative and quantitative studies, it was found that the TiO_2 NTs' surface has amphiphilic properties. Therefore, a self-cleaning capability associated with the amphiphilic and the photocatalytic properties can be achieved on the surface of TiO_2 NT arrays prepared through electrochemical oxidization.

4. Conclusions

During the electrochemical oxidation of Ti, there exist 4 stages for making well-ordered TiO_2 NTs. In the first stage, when the potential is very low, oxygen formation and Ti dissolution are the major reactions. The second stage corresponds to a slightly higher potential, but less than 2.5 V. In this stage, the formation of TiO_2 film occurs. When the potential is increased to the even higher range from 2.5 V to 6 V, the TiO_2 film dissolves and nanoporous surface structure is generated. This belongs to the third stage. Further increase of the potential enters stage four. The high potentials cause the self-organization of the nanostructure and allow the formation of well-aligned TiO_2 NTs. It is also found that the change in surface condition of Ti by annealing heat treatment affects the surface oxide film dissolution kinetics. The well-ordered TiO_2 NTs synthesized by electrochemical oxidation exhibit a stronger photocatalytic activity than the TiO_2 film. It is a good photo-catalyst for decomposition of organic materials. The surface of the TiO_2 NTs has amphiphilic properties. Both water and oil can wet the surface of TiO_2 NT arrays due to the capillary effect of the nanotubes. This self-cleaning property is expected on the surface with TiO_2 NT arrays based on both its amphiphilic properties and high photo-catalytic activity. UV light excites electrons on the surface of TiO_2 NT arrays and radicals are generated to decompose organic matters.

Acknowledgements

This work is supported by the research start-up fund, the Faculty Summer Research Fellowship and the Doctoral Instrumentation Graduate Fellowship from The University of Toledo. We appreciate the editor, Dr. Hongge Pan, and the anonymous reviewers for the valuable suggestions on modifying the paper.

References

[1] A. Fujishima, K. Honda, Nature 238 (1972) 37–38.
[2] M.A. Gondal, M.N. Sayeed, A. Alarfaj, Chem. Phys. Lett. 445 (2007) 325–330.
[3] Y. Li, W. Xie, X. Hu, G. Shen, X. Zhou, Y. Xiang, X. Zhao, P. Fang, Langmuir 26 (2010) 591–597.
[4] K. Vinodgopal, I. Bedja, P.V. Kamat, Chem. Mater. 8 (1996) 2180–2187.
[5] F. Zhang, S.S. Wong, Chem. Mater. 21 (2009) 4541–4554.
[6] A. Chabas, T. Lombardo, H. Cachier, M.H. Pertuisot, K. Oikonomou, R. Falcone, M. Verita, F. Geotti-Bianchini, Build. Environ. 43 (2008) 2124–2131.
[7] C. Euvananont, C. Junin, K. Inpor, P. Limthongkul, C. Thanachayanont, Ceram. Int. 34 (2008) 1067–1071.
[8] M.A. Tony, Y.Q. Zhao, P.J. Purcell, M.F. El-Sherbiny, J. Environ. Sci. Health Part A 44 (2009) 488–493.
[9] L. Peruchon, E. Puzenat, J.M. Herrmann, C. Guillard, Photochem. Photobiol. Sci. 8 (2009) 1040–1046.
[10] L. Zhang, Y. Zhu, Y. He, W. Li, H. Sun, Appl. Catal. B: Environ. 40 (2003) 287–292.
[11] K. Shankar, G.K. Mor, H.E. Prakasam, S. Yoriya, M. Paulose, O.K. Varghese, C.A. Grimes, Nanotechnology 18 (2007) 065707.
[12] L.K. Tan, M.K. Kumar, W.W. An, H. Gao, ACS Appl. Mater. Interface 2 (2010) 498–503.
[13] S. Zhang, J. Zhou, Z. Hang, Z. Du, A.V. Vorontsov, Z. Jin, Chin. Sci. Bull. 45 (2000) 1533–1536.
[14] S. Yang, Y. Liu, C. Sun, Appl. Catal. A 301 (2006) 284–291.
[15] X. Wu, Q. Jiang, Z. Ma, M. Fu, W.F. Shangguan, Solid State Commun. 136 (2005) 513–517.
[16] S. Srimala, C.W. Lai, J. Alloys Compd. 490 (2010) 436–442.
[17] S.I. Na, S.S. Kim, W.K. Hong, J.W. Park, J. Jo, Y.C. Nah, T. Lee, D.Y. Kim, Electrochim. Acta 53 (2007) 2560–2566.
[18] G.K. Mor, O.K. Varghese, M. Paulose, K. Shankar, C.A. Grimes, Solar Energy Mater, Sol. Cells 90 (2006) 2011–2075.
[19] V. Zwilling, E. Darque-Ceretti, A. Boutry-Forveille, D. David, M.Y. Perrin, M. Aucouturier, Surf. Interface Anal. 27 (1999) 629–637.
[20] C.C. Chen, J.S. Lin, E.W. Diau, T.Z. Liu, Appl. Phys. A 92 (2008) 615–620.
[21] M. Bestetti, S. Franz, M. Cuzzolin, P. Arosio, P.L. Cavallotti, Thin Solid Films 515 (2007) 5253–5258.
[22] K. Bauer, S. Kleber, P. Schmuki, Electrochem. Commun. 8 (2006) 1321–1325.
[23] H. Yang, C. Pan, J. Alloys Compd. 492 (2010) L33–L35.
[24] D.J. Yang, H. Park, H.G. Kim, S.J. Cho, W.Y. Choi, J. Electroceram. 23 (2009) 159–163.
[25] J.M. Macak, P. Schmuki, Electrochim. Acta 52 (2006) 1258–1264.
[26] Z. Zhang, M.F. Hossai, T. Takahashi, Int. J. Hydrogen Energy 35 (2010) 8528–8535.
[27] J. Guo, W. Fu, H. Yang, Q. Yu, W. Zhao, X. Zhou, Y. Sui, J. Ding, Y. Li, S. Cheng, M. Li, J. Phys. D: Appl. Phys. 43 (2010) 245202.
[28] A. Ghicov, H. Tsuchiya, J.M. Macak, P. Schmuki, Electrochem. Commun. 7 (2005) 505–508.
[29] J.M. Macak, K. Sirotna, P. Schmuki, Electrochim. Acta 50 (2005) 3679–3684.
[30] S. Sreekantan, Z. Lockman, R. Hazan, M. Tasbihi, L.K. Tong, A.R. Mohamed, J. Alloys Compd. 485 (2009) 478–483.
[31] Z. Lockman, S. Sreekantan, S. Ismail, L. Schmidt-Mende, J.L. MacManus-Driscoll, J. Alloys Compd. 503 (2010) 359–364.
[32] J. Zhao, X. Wang, T. Sun, L. Li, J. Alloys Compd. 434–435 (2007) 792–795.
[33] Y.Y. Song, F. Schmidt-Stein, S. Bauer, P. Schmuki, J. Am. Chem. Soc. 131 (2009) 4230–4232.
[34] A.G. Munoz, Electrochim. Acta 52 (2007) 4167–4176.
[35] Y. Tang, J. Tao, Y. Zhang, T. Wu, H. Tao, Z. Bao, Acta Phys. Chim. Sinica 24 (2008) 2191–2197.